International Journal of Heat and Mass Transfer 52 (2009) 4785–4795

Contents lists available at ScienceDirect

International Journal of Heat and Mass Transfer

journal homepage: www.elsevier.com/locate/ijhmt

Numerical studies on the combustion properties of char particle clusters

Xiang Jun Liu *, Li Li

Thermal Engineering Department, University of Science and Technology of Beijing, Beijing 100083, China

ARTICLE INFO

Article history:
Received 27 September 2008
Received in revised form 10 June 2009
Accepted 12 June 2009
Available online 17 July 2009

Keywords:
Char particle cluster
Char combustion
Numerical studies

ABSTRACT

Particle clustering is an important phenomenon in dense particle–gas two-phase flow. One of the key problems worth studying is the reacting properties of particle clusters in coal particle combustion process in the dense particle region. In this paper, a two-dimensional mathematical model for the char cluster combustion in airflow field is established. This char cluster consists of several individual particles. The comprehensive model includes mass, momentum, and energy conservation equations for both gas and particle phases. Detailed results regarding velocity vector, mass component, and temperature distributions inside and around the cluster are obtained. The micro-scale mass and heat transfer occurred inside and around the char cluster are revealed. By contrastively studying the stable combustion of char particle clusters consisting of different particles, the combustion properties of char clusters in various particle concentrations are presented and discussed.

1. Introduction

Coal particle combustion is a two-phase reaction process, and the local particle–gas two-phase heat transfer and the mass transfer processes determine the coal combustion properties. The coal combustion properties in dilute particle regions, where the coal particle behaves independently, have been extensively studied by experimental and numerical methods [1,2]. In practical applications, the global or local particle concentration in a combustor is generally high, therefore the particle interaction has significant impacts on the combustion process. In these cases, the well known combustion properties of an isolated coal particle are not applicable to interaction-dominated coal particle combustion in dense particle regions [3].

In interaction-dominated coal particle combustion, most particles are presented as a cluster or a cloud surrounded by a diffusion flame. This phenomena is different from that in dilute-suspension pulverized coal boilers, and was observed and verified by lots of experimental and theoretical studies [4–7].

Particle clustering is an important phenomenon in dense particle–gas two-phase flow [8]. It means that groups of several to dozens of particles are congregated in the flow field due to complex particle–particle and particle–gas interactions. Motions and heterogeneous reactions of particles are presented as particle-cluster moving and particle-cluster-gas reactions [9,10]. The key problem in coal particle combustion process at dense particle regions is to study the combustion characteristics of coal particle clusters.

Several mathematical models have been developed to study the coal cluster combustion characteristics in the last two decades. Annamalai and Ryan [11,12] proposed a spherical cloud model to study coal cloud combustion, and the results indicate that the particle interaction had a significant effect on ignition and char combustion. Using a transient group combustion model, Du et al. [13] studied the combustion process for a cylindrical cloud of pulverized coal particle. The effects of particle density, particle size, and cloud radius on ignitions were investigated. Recently, a 1-D model for coal particle cluster combustion under quiescent conditions was proposed by Shuyan et al. [14]. The impacts on ignition and combustion of coal particle cluster by radiative heat transfer, group number, ambient temperature, coal particle size, and oxygen concentration were studied. These simulation studies are very helpful to understand the coal cluster properties. However, all these existing models treat the coal cluster or cloud as a uniform continuity porous phase. Mathematically, the complex interactions of particle to particle and particle to gas are taken into account by introducing the gas volume fraction ε in the cluster. This simplification is difficult to obtain a deep insight into the combustion process of coal clusters. To gain a fundamental understanding of the coal cluster combustion behavior, the key problem is to study the micro-scale mass and heat transfer processes occurred inside and around coal clusters. Unfortunately, the size of coal clusters to be considered in the complex local two-phase flow is generally less than 1–2 cm [10], and few literatures exist on either experimental or numerical studies on these micro-scale mass and heat transfer processes.

Char combustion process is an important part of coal cluster combustion. The time required to burn-out char is much longer than that required for vaporization or pyrolysis. In this paper, the combustion properties of char clusters are numerically studied.

* Corresponding author. Tel.: +86 10 62333792.
E-mail address: liuxj@me.ustb.edu.cn (X.J. Liu).

0017-9310/$ - see front matter © 2009 Elsevier Ltd. All rights reserved.
doi:10.1016/j.ijheatmasstransfer.2009.06.009

Nomenclature

C_p	gas specific heat, kJ/(kg K)	T_c	char temperature, K
D_l	diffusion coefficient of species l, m^2/s	T_∞	environmental temperature, K
d	particle diameter, m	u_i	gas velocity, m/s
$\vec{n}_s$	surface normal vector of char particle	u_∞	environmental gas velocity, m/s
M_l	molecule weight of species l, kg/mol	Y_l	mass fraction of species l
M_c	molecule weight of char, kg/mol	$Y_{l\infty}$	environmental mass fraction of species l
P	pressure, Pa	λ	thermal conductivity of gas phase, kJ/(m s K)
Q_n	heat produced by gas reaction n, kJ/kg	λ_c	thermal conductivity of solid char, kJ/(m s K)
Q_R	radiative heat, kJ/(m^3 s)	μ	fluid viscosity, Pa s
Q_k	heat produced by heterogeneous reaction k, kJ/kg	ρ	fluid density, kg/m^3
R_n	rate of gas reaction n, mol/(m^3 s)	ρ_c	char density, kg/m^3
$R_{s,k}$	rate of heterogeneous reaction k at surface s, mol/(m^2 s);	ω_l	the mass production rate of species l from chemical reactions, kg/(m^3 s)
T	gas temperature, K		

Rather than treating the char cluster as a continuity porous phase, a char cluster consisting of several individual particles is considered. The two-dimensional mathematical model of char cluster combustion in airflow field, which is derived from mass, momentum, and energy conservation law, is established. In order to study the effects of particle concentration on cluster combustion properties, six typical cluster combustion cases with different number of inner particles are simulated. Detailed results of these six cases regarding velocity vector, mass component, and temperature distributions inside and around the clusters are obtained, and these results reveal the details of the micro-scale mass and heat transfer processes occurred inside and around the char clusters. Finally, the combustion properties of char clusters in various particle concentrations are studied and discussed.

2. Mathematical model

The computational domain and boundary conditions are shown in Fig. 1. For purpose of simplification, a 2-D steady combustion process is studied. The char cluster is assumed to be quiescent in a steady high-temperature air flow. It consists of several individual char particles. The diameter of a single particle d is 100 μm and the diameter of a cluster is 9d. According to the relations between calculation accuracy and the size of the computational domain [15], we adopted a $270d \times 180d$ rectangle domain which is sufficient for the calculation accuracy in this paper.

2.1. Governing equations

For most of the real cases, the gas-cluster slip velocity in dense coal particle–gas two-phase flow is very slow and the particle

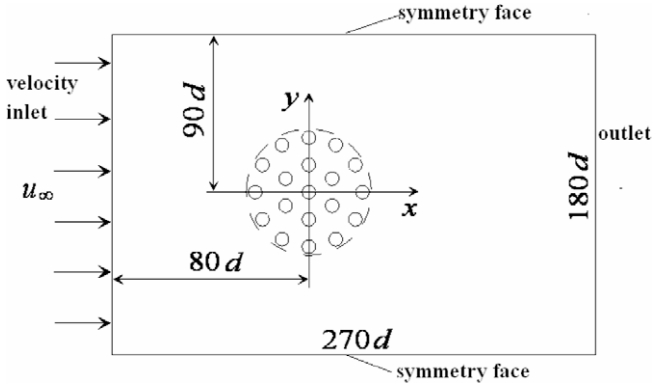

Fig. 1. Schematic diagram of the cluster and computational domain.

Reynolds number $Re_p = \rho u d/\mu$ (where u is the slip velocity, d is the particle diameter, μ is the fluid viscosity, and ρ is the fluid density) is limited in a small range. The particle Reynolds number used in present work is about 0.12. Therefore, the flow calculated here can be considered as a steady incompressible laminar one and the governing equations of mass, momentum, species and energy in 2-D Cartesian coordinates can be written in the following forms:

$$\text{Continuity equation}: \quad \frac{\partial}{\partial x_j}(\rho u_j) = \sum \omega_l \tag{1}$$

$$\text{Momentum equation}: \quad \frac{\partial}{\partial x_j}(\rho u_j u_i) = -\frac{\partial P}{\partial x_i} + \frac{\partial}{\partial x_j}\left(\mu \frac{\partial u_i}{\partial x_j}\right) \tag{2}$$

$$\text{Species equation}: \quad \frac{\partial}{\partial x_j}(\rho u_j Y_l) = \frac{\partial}{\partial x_j}\left(\rho D_l \frac{\partial Y_l}{\partial x_j}\right) + \omega_l \tag{3}$$

where D_l and Y_l are the diffusion coefficient and the mass fraction of species l; ω_l is the mass production rate of the species from chemical reactions. The subscript l = O, F, P, N, represent species of O_2, CO, CO_2, and N_2, respectively.

$$\text{Energy equation of gas phase}: \quad \frac{\partial}{\partial x_j}(\rho u_j C_p T) = \frac{\partial}{\partial x_j}\left(\lambda \frac{\partial T}{\partial x_j}\right) + \sum_n M_l R_n Q_n + Q_R \tag{4}$$

where C_p and λ are the specific heat capacity and thermal conductivity of gas phase; M_l is the molecule weight of species l; R_n is the reaction rate of gas reaction n; Q_n is the heat produced by gas reaction n; Thus, $\sum_n M_l R_n Q_n$ expresses the heat produced as a result of chemical reaction in the gas phase; Q_R is the radiative heat.

In this study, the effects of interior pore structures in char combustion are neglected. The char particles only burn at the surface areas, thus there is no reaction heat inside the solid phase.

$$\text{Energy equation of solid phase}: \quad \frac{\partial}{\partial r}\left(\lambda_c r \frac{\partial T_c}{\partial r}\right) + \frac{1}{r}\frac{\partial}{\partial \theta}\left(\lambda_c \frac{\partial T_c}{\partial \theta}\right) = 0 \tag{5}$$

where λ_c and T_c are the thermal conductivity and temperature of solid char. The energy equation of solid phase is written in cylindrical coordinates which is preferable for studying char cluster heat transfer process.

2.2. Combustion model

The combustion reactions considered in this paper include Char–O_2 reaction, Char–CO_2 reaction, and CO–O_2 homogeneous reaction. Products of Char–O_2 reaction are CO and CO_2. However,

Table 1
Reaction rates used in the simulation.

Reaction	Reaction rate	Reaction rate constant	Reaction heat kJ/mol	References
I	$R_I = K_I C_{O_2}$ (mol m^{-2} s^{-1})	$K_I = 1.9 \times 10^7 \exp(-23815/T)$	2.21×10^2	[20,22]
II	$R_{II} = K_{II} C_{CO_2}$ (mol m^{-2} s^{-1})}	$K_{II} = 1.291 \times 10^5 \exp(-22976/T)$	-1.73×10^2	[20,21]
III	$R_{III} = K_{III} C_{CO} C_{O_2}^{1/2}$ (mol m^{-3} s^{-1})	$K_{III} = 1.3 \times 10^8 \exp(-15094/T)$	5.56×10^2	[21,23]

Where $C_{O_2}, C_{CO_2}, C_{CO}$ are mole concentration of O_2, CO_2, and CO (mol m^{-3}).

experimental results show that $[CO]/[CO_2] = 2500 \exp(-6249/T)$ [16] which implies the content of CO_2 is much less and could be neglected when temperature is higher. In this paper, we consider the production of CO only. The reaction rates used in present simulations are listed in Table 1:

$$2C + O_2 \rightarrow 2CO \quad \text{(I)}$$
$$C + CO_2 \rightarrow 2CO \quad \text{(II)}$$
$$2CO + O_2 \rightarrow 2CO_2 \quad \text{(III)}$$

2.3. Boundary conditions

As shown in Fig. 1, the environmental gas velocity u_∞, species $Y_{l\infty}$, and temperature T_∞ are set to be same as those under free stream conditions. The inlet is in a uniform distribution. The fully developed flow is taken as the outlet condition. Other faces are symmetrical boundaries.

No-slip velocity condition and local mass and heat balance conditions are employed at the interfaces between the particle and the gas:

$$\begin{aligned} &\vec{u}_j = 0 \\ &\omega_{s,j} = -(\rho D_l \nabla Y_l)_s \cdot \vec{n}_s \\ &\sum_k M_c R_{s,k} Q_k = -(\lambda \nabla T)_s \cdot \vec{n}_s + \left(\lambda_c \frac{\partial T_c}{\partial r}\right)_s + Q_{s,r} \end{aligned} \quad (6)$$

where $\vec{n}_s$ is the surface normal vector; $\sum_k M_c R_{s,k} Q_k$ is the heat flux rate produced by heterogeneous reactions; $Q_{s,r}$ is the radiative heat flux rate of the particle surface.

3. Method of solution

It is well known that an efficient computational grid system is important for a simulation work because it impacts the accuracy and convergence of flow solution. Considering the geometrical complexity of the simulation domain shown in Fig. 1, a combined structured and unstructured grid system is adopted in this simulation. As shown in Figs. 2 and 3, a non-uniform Delaunay Triangulation unstructured mesh [17] with more nodes accumulated around the particles is used for discretizing the governing equations of gas phase. The gas mesh size inside or near the cluster is in the range from 5 to 13 μm, or 1/20 to 1/8 of the particle diameter. This grid is sufficient to accurately capture micro-scale mass and heat transfer processes occurred inside and around the char cluster. The structured grid in cylindrical coordinates is adopted for solid phase. As shown in Fig. 4, the node number of each individual particle is 36×5.

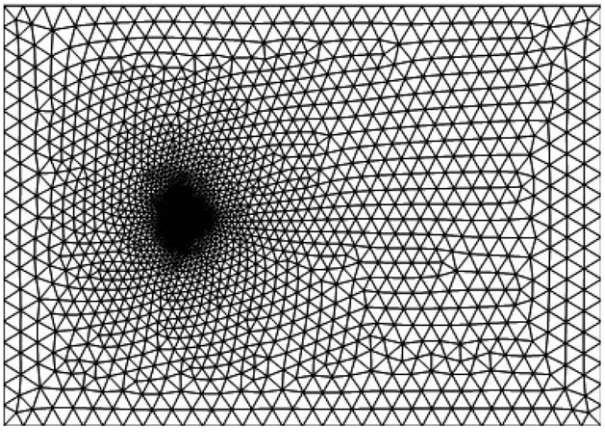

Fig. 2. Grid system of computational domain.

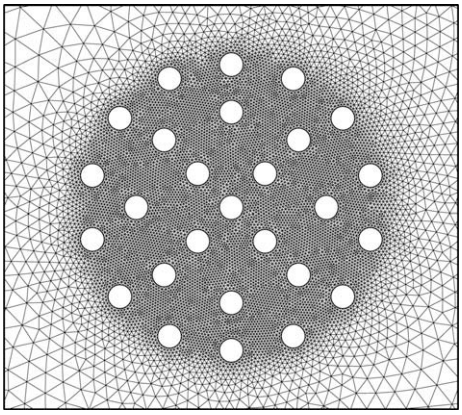

Fig. 3. Mesh distribution near and inside the cluster.

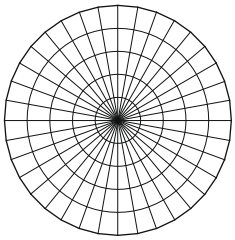

Fig. 4. Mesh distribution for a particle.

In this grid system, both the governing equations of gas phase and solid phase are discretized by finite volume method [18]. The power-low scheme is used for the convective and diffusive flux terms to overcome the numerical diffusion as well as to obtain the accurate flow field. The SIMPLE algorithm is used to resolve the coupling between velocity and pressure [19]. The radiative heat transfer process is modeled using the Monte Carlo Method.

4. Calculated results

We consider a char cluster consisting of several individual particles located in a steady high-temperature air flow. The diameter of a single particle is d and the diameter of the cluster is $9d$. In order to study the effects of particle concentration on cluster combustion properties, as shown in Fig. 5a–f, six cases with particle

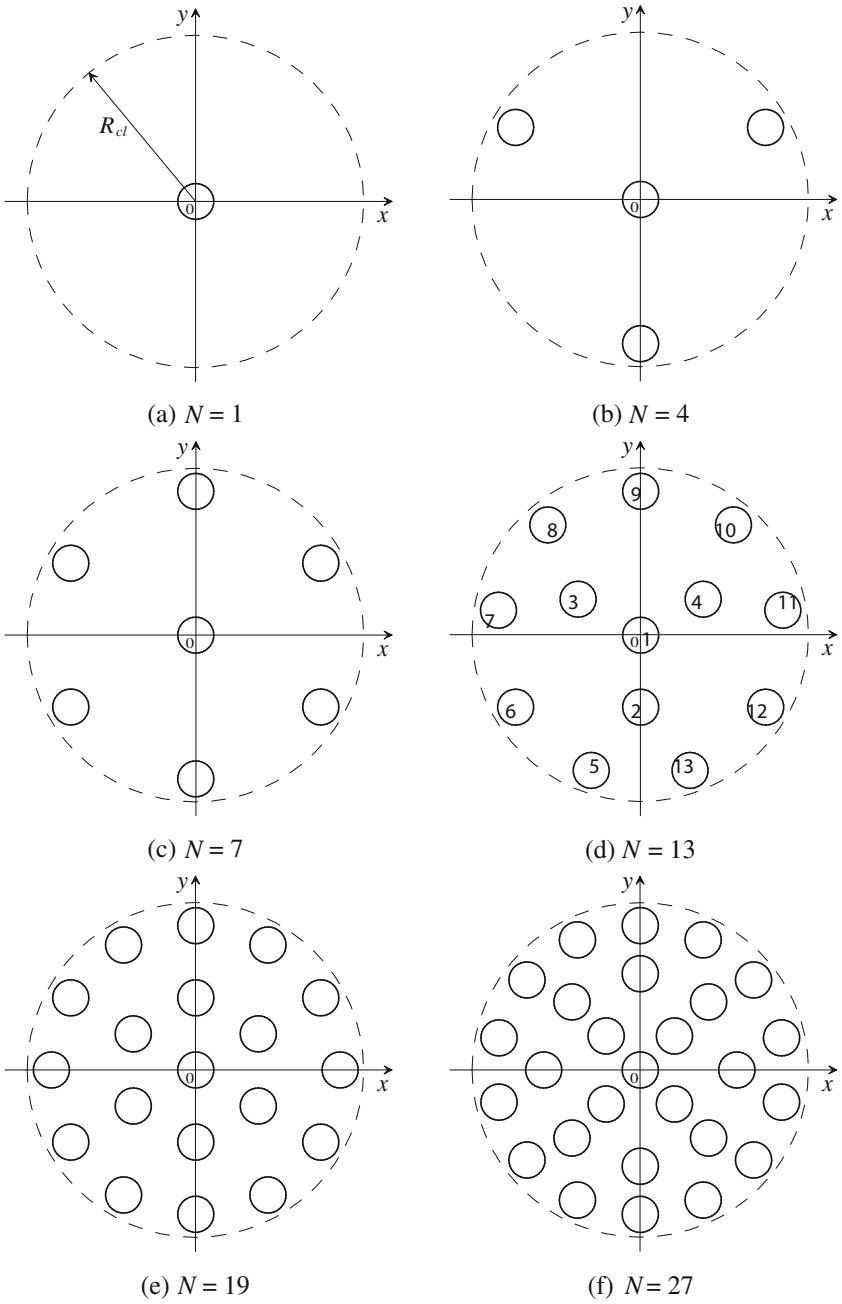

Fig. 5. Physical configurations of char particles inside the clusters.

number N taking the value 1, 4, 7, 13, 19, and 27 are simulated, respectively. The corresponding particle concentration of each cluster is 0.0123, 0.0494, 0.0864, 0.1605, 0.2346, and 0.3333. The parameters used in the present simulation are listed in Table 2.

Table 2
Parameter settings.

Particle diameter	$d = 100$ μm
Cluster diameter	$D = 9d = 900$ μm
Computational domain	$270d \times 180d = 27 \times 18$ mm
Velocity of incoming gas flow	$u_\infty = 0.2$ m/s
Gas temperature of incoming gas	$T_\infty = 1273$ K
Gas pressure at ambient	$P_\infty = 1.01 \times 10^5$ Pa
Oxygen of incoming gas	$Y_{O,\infty} = 0.233$
Nitrogen of incoming gas	$Y_{N,\infty} = 0.767$
Apparent emissivity of char particle	$\varepsilon = 0.8$
Thermal conductivity of char particle	$\lambda_c = 1.92$ W/(m K)
Laminar gas viscosity at 0 °C	$V_0 = 1.32 \times 10^{-6}$ m^2/s
Gas density at 0 °C	$\rho_0 = 1.293$ kg/m^3

4.1. Gas velocity vectors nearby and inside the clusters

Fig. 6a–f illustrates the calculated gas velocity vectors nearby and inside the clusters. The incoming velocity is 0.2 m/s and $Re_p = \rho u d/\mu \approx 0.12$. Since the inertia effects are negligible, there is no separation of boundary layer occurred at the particle surfaces. The flow pattern is nearly symmetric and similar to that of an ideal flow. The velocity inside the cluster in any cases is very low compared with the incoming velocity, and decreases rapidly when the number of particles increases. For example, when the number of particles is 4, the maximum gas velocity inside the cluster is 0.036 m/s, while it decreases to 0.014, 0.0046, 0.0022, and 0.00041 m/s when the number of particles is 7, 13, 19, and 27,

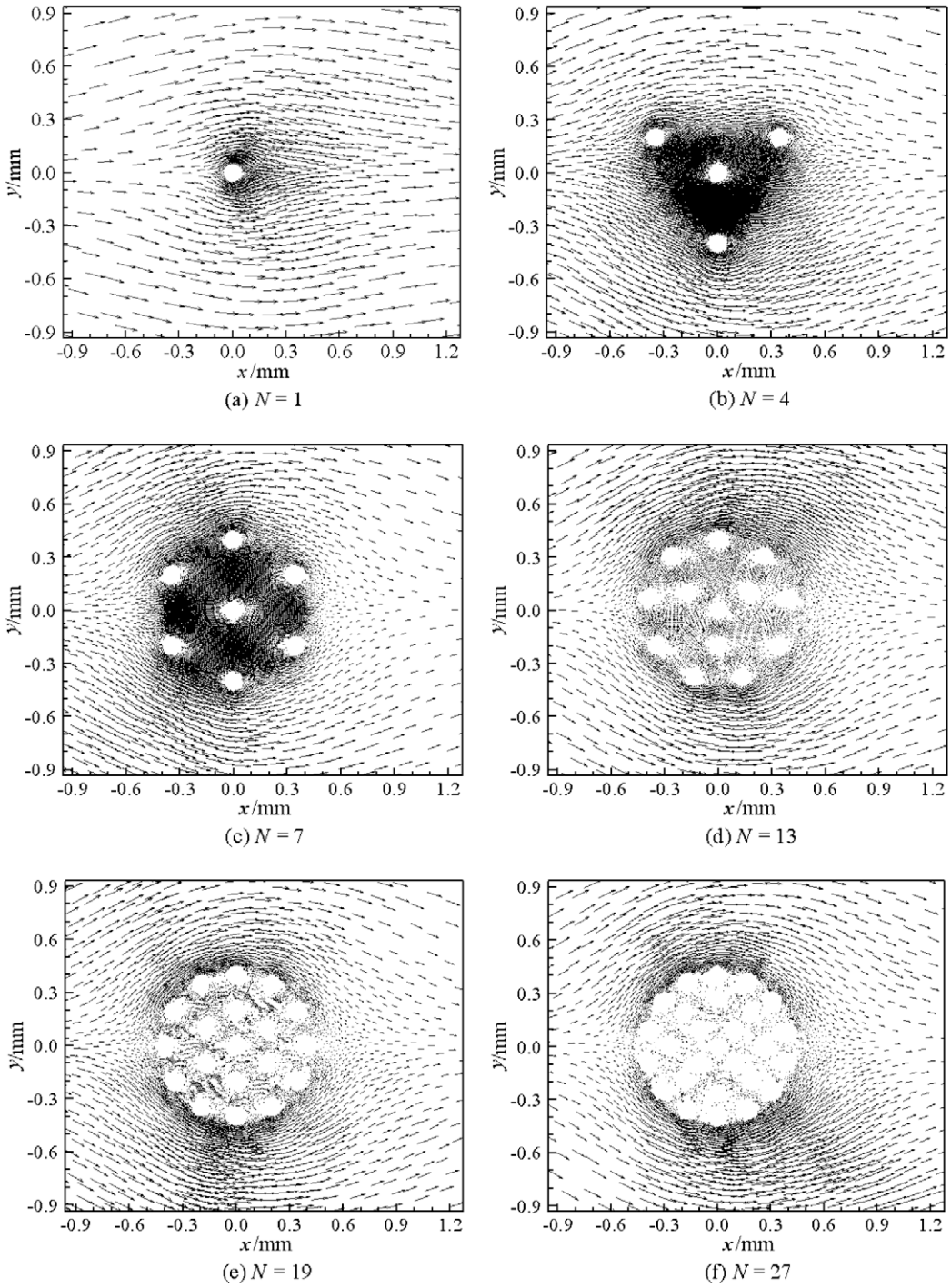

Fig. 6. (a–f) Calculated gas velocity vectors around the clusters.

respectively. This implies that the air flow inside the cluster can be neglected when the particle concentration is high.

4.2. O_2 and gas temperature distributions nearby and inside the cluster

Fig. 7a and b show the O_2 (mass fraction) and the gas temperature distributions around the cluster at $N = 1$. These two figures show the typical combustion characteristics of a single char particle placed in a hot oxidizing atmosphere. The char is oxidized to CO at the particle surface, and then CO is oxidized, forming the CO flame region surrounding the particle. As a consequence, the O_2 mass fraction decreases toward the particle and reaches zero value at the particle surface, while the temperature increases toward the particle and reaches peak value near the particle surface. Because of the convection effects of the downstream along x direction, both the O_2 mass concentration and the temperature distributions are asymmetric along x direction, and the maximum temperature region occurs at the rear of the particle. The temperature difference between particle and flame caused by the combustion of CO is up to 500 K.

Fig. 8a and b show the O_2 mass concentration and the temperature distributions around the cluster at $N = 4$. In this case, the mean distance between any two particles is $4d$. O_2 and other species in the boundary layer of a char particle may be influenced by

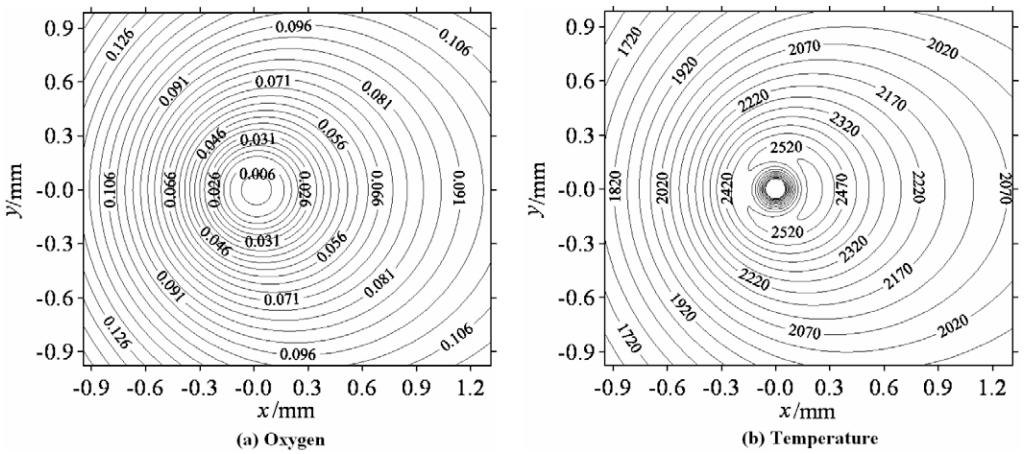

Fig. 7. (a and b) O_2 and the temperature distributions around the cluster for $N = 1$.

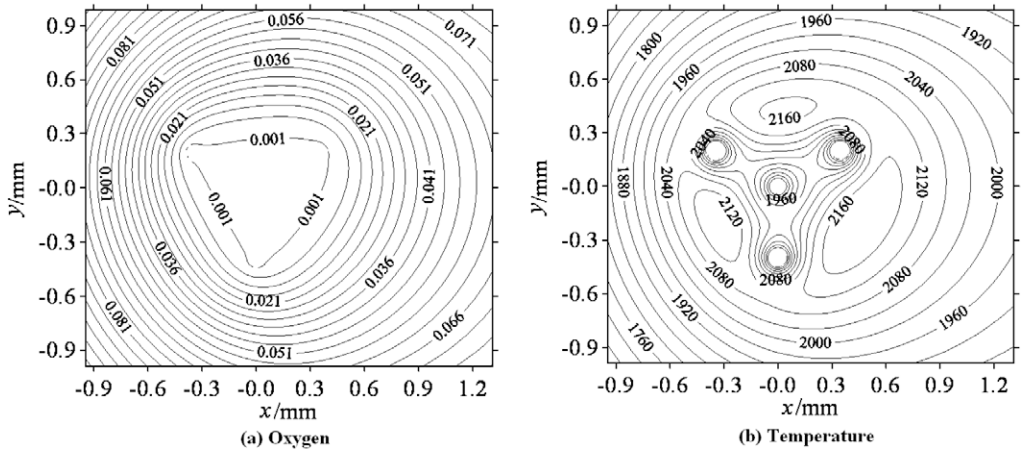

Fig. 8. (a and b) O_2 and the temperature distributions around the cluster for $N = 4$.

other particles nearby. The local mass and heat transfer processes of any char are different from those of an isolated particle. As shown in Fig. 8a, the 0.001 contour line of O_2 mass concentration forms a triangle around the outer three particles. This indicates that most O_2 is depleted by the outer three particles. However, each particle inside the cluster still burns with its individual flame front in this case. Annamalai and Ryan [12] presented a comprehensive theoretic analysis on the interactive char combustion process. Based on the simultaneous analysis of inner transport rate and outer cluster-gas transport rate, they proposed that as the number of particles per unit volume increases continuously, the char particle behaves sequentially, first as an isolated particle combustion with individual flame combustion, then as a partial group combustion, and finally as a sheath combustion. Adopting this classification, Char cluster combustion of $N = 4$ can be called as individual flame combustion.

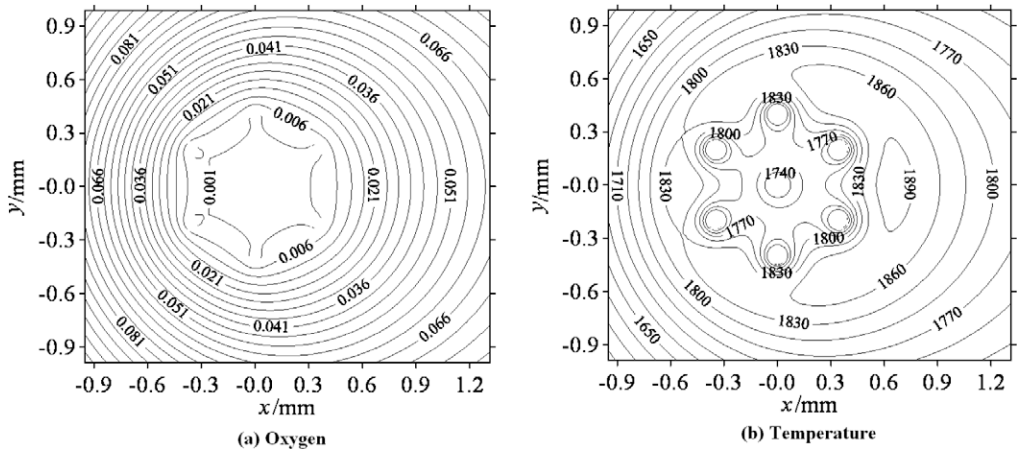

Fig. 9. (a and b) O_2 and the temperature distributions around the cluster for $N = 7$.

Fig. 9a and b show the O_2 mass concentration and the temperature distributions around the cluster at $N = 7$. In this case, the particle concentration of the cluster is 0.0864. As shown in Fig. 5c, there are six particles located in the outer circle, while the distance between the outer particles and the center particle is the same as that of $N = 4$. Due to the increase of the particles, O_2 is further depleted by the outer six particles. The contour lines of O_2 mass concentration of the outer six particles overlap and form a hexagon. Similar to that of $N = 4$, each particle still burns with its individual flame front in this case. Furthermore, from Figs. 6b to 9b, we can

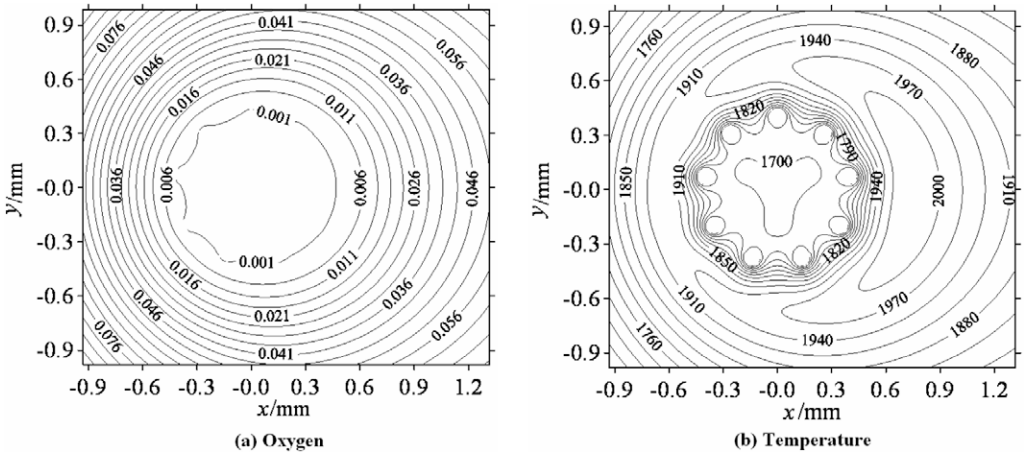

Fig. 10. (a and b) O_2 and the temperature distributions around the cluster for $N = 13$.

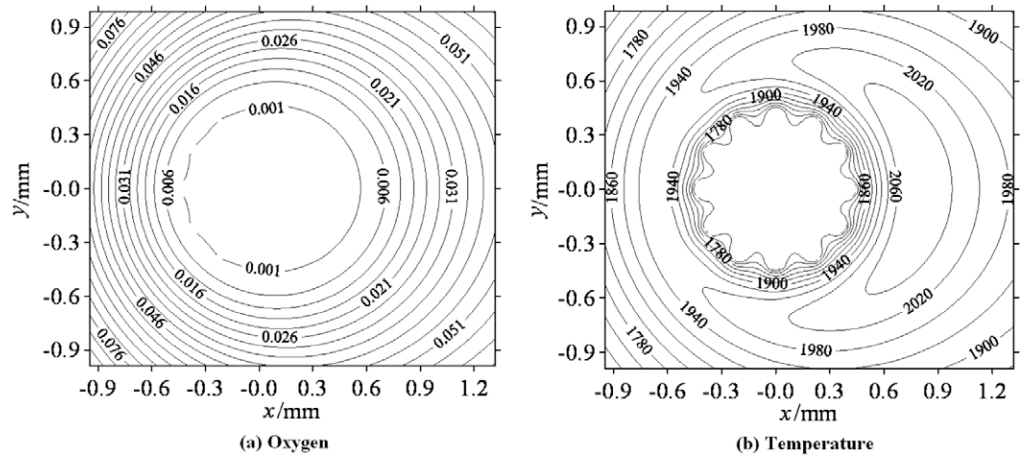

Fig. 11. (a and b) O_2 and the temperature distributions around the cluster for $N = 19$.

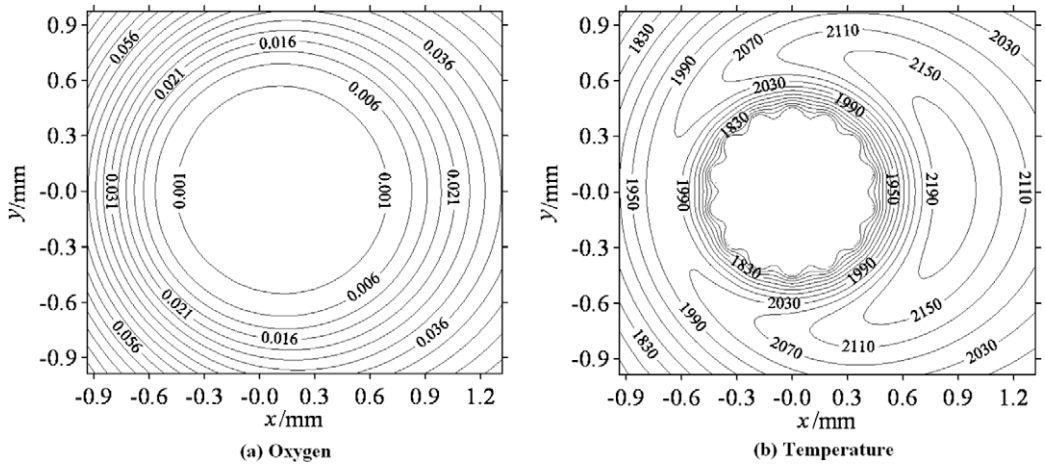

Fig. 12. (a and b) O_2 and the temperature distributions around the cluster for $N = 27$.

find that when the number of particles is not more than 7, both the flame temperature and particle temperature decrease as the particles increase.

As shown in Fig. 5d, 12 particles are located in two circles around the central char particle for the cluster with $N = 13$. Fig. 10a and b show the O_2 mass concentration and the temperature distributions around the cluster at $N = 13$. The nine particles located at the outer circle still burn individually, but the flame fronts expand and contact with the neighbor particles'. The inner four particles form a triangle flame around them. This is because that there is only deoxidization reaction of CO_2 to CO inside the cluster due to the lack of O_2, which is exhausted by outer nine particles of the cluster. The CO, produced by this deoxidization reaction, diffuses outward and forms the inner group combustion flame. This combustion type can be called as partial group combustion.

When particles inside a cluster increase to 19 or 27, the particle concentration of each cluster is up to 0.2346 or 0.3333, respectively. As shown in Figs. 11 and 12, the production and burning rate of CO of the outer particles are much faster, which results in that the O_2 could not diffuse into the cluster and the flame only forms at the cluster surface. The gas temperature is nearly the same inside the cluster, and the gas temperature surrounding the cluster surface is the flame temperature. Further analyses show that the temperature difference among each particle inside the cluster is less than 0.3 °C. The Char cluster behaves as a single large particle with pore surface. The combustion under this mode can be called as group combustion.

4.3. Species and gas temperature profiles along x direction

The more detailed distributions of species and temperature are shown in Figs. 13–16. Fig. 13a and b show the O_2 mass concentration profiles along x direction at $y = 0$ section. Consistent with O_2 contours at different cases shown in Figs. 7a–12a, as the number of particles inside the cluster increases, the consumption of O_2 becomes faster, thus the O_2 mass fraction near and inside the cluster decreases rapidly, and the zero value region of O_2 enlarges.

Fig. 14a and b show the CO mass concentration profiles along x direction at $y = 0$ section. CO is concentrated at the region of -0.6 mm $< x <$ 0.6 mm (cluster region: -0.45 to 0.45 mm), where the heterogeneous and homogeneous reactions are taken placed. When the number of particles is not more than 7, the O_2 supplied by the bulk gas is sufficient for char combustion. The heterogeneous reaction of the coal particle cluster depends mainly upon reaction I. Therefore, as shown in Fig. 14a, with the number of par-

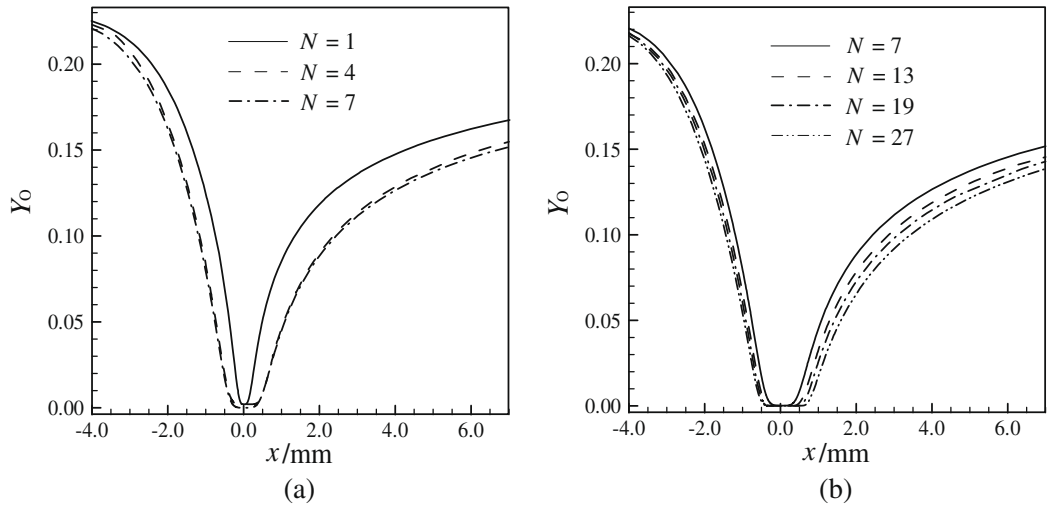

Fig. 13. O_2 profiles along x direction at $y = 0$.

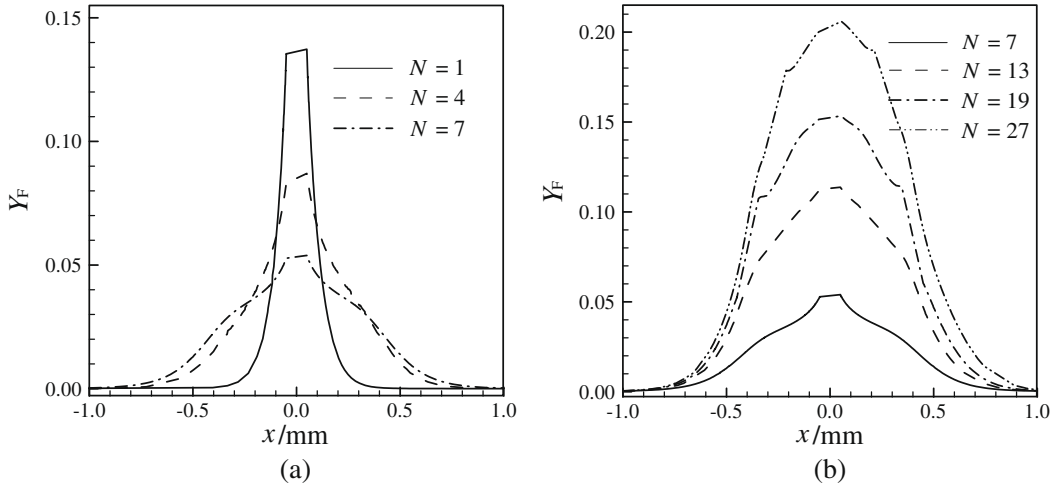

Fig. 14. CO profiles along x direction at $y = 0$.

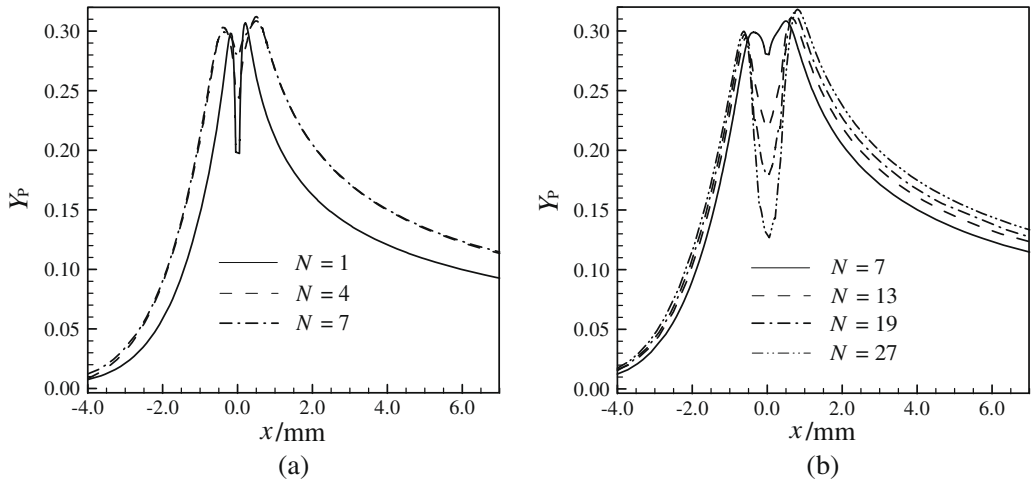

Fig. 15. CO_2 profiles along x direction at $y = 0$.

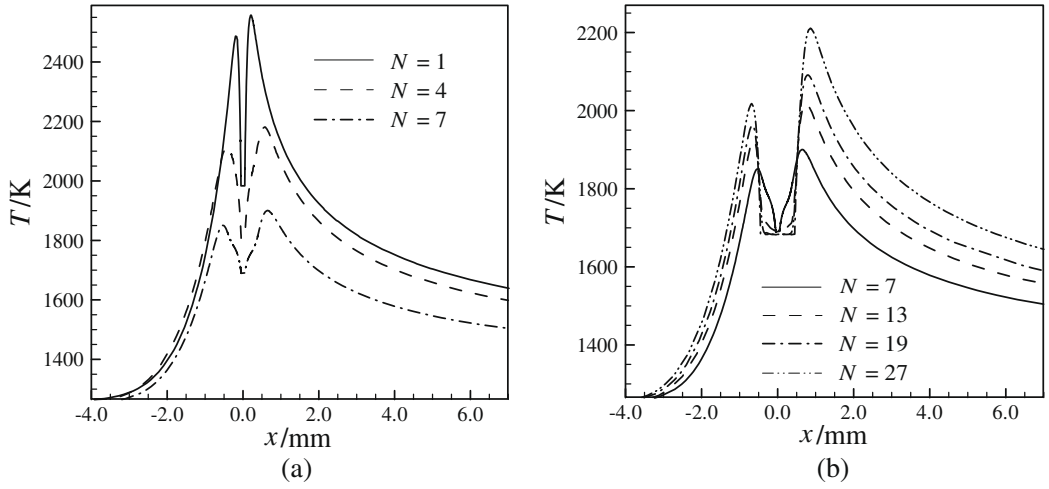

Fig. 16. Temperature profiles along x direction at $y = 0$.

ticles increasing from $N = 1$ to $N = 7$, the inner CO mass concentration decreases due to the lack of O_2, while the CO mass concentration at the outer layer of the cluster increases due to the increases of total char amount. However, this trend reverses when the number particles increases further. As shown in Fig. 14b, when particles are more than 7, the reaction rate of reaction II increases. There are more deoxidization reactions of CO_2 to CO inside the cluster due to the lack of O_2. Thus, the production amount and reaction rate of CO increase with the increase of particles.

Fig. 15a and b show the CO_2 mass concentration profiles along x direction at $y = 0$ section. There are two separated CO_2 peaks at x direction which means a gas flame is formed around the cluster center. The higher peak located at the rear region due to the convection effects of downstream. As the number of particles increases, the distance and the temperature difference between the two peaks increase. This means the cluster flame front expands and the combustion at the rear region is intensified as the particles increase.

Fig. 16a and b show the temperature profiles along x direction at $y = 0$ section. There are also two separated temperature peaks occurred around the cluster center. From Figs. 13–16, there are strong coherence among the CO_2 peak shapes in Fig. 15, temperature peak shapes in Fig. 16, O_2 valley shapes in Fig. 13, and CO valley shapes in Fig. 14. When the number of particles is not more than 7, as shown in Fig. 16a, both the global gas temperature and the temperature difference between the peak and the valley decrease with the particles increase; when the number of particles is more than 7, the deoxidization reaction of reaction II becomes dominative reaction inside the cluster. Therefore, as the particles increase, the production of CO increases, and CO combustion around the cluster is intensified. Then, the flame temperature increases and the flame front expands. At the same time, the inside temperature becomes uniformly distributed as the particles increase.

4.4. Particle temperature and burning rates

As mentioned above, the node number of each individual particle is 36×5. The temperature inside each individual particle is investigated in detail. However, the calculated results show that both the inner temperature difference inside a single particle and the temperature difference among particles are very small in all the simulation cases. The mean temperature of each particle at case of $N = 13$ are listed in Table 3. The location of each particle is marked in Fig. 5d. The temperature of particle 1 which is located at the cluster center is the lowest, but the temperature differences among particles are less than 0.3 K in this case. Fig. 17 shows the mean temperature variation of the center particle with different

Table 3
Particle temperature and burning rate of each particle at the case of $N = 13$.

Particle location	1	2	3	4	5	6
Temperature (K)	1694.9	1694.9	1694.9	1694.9	1695.2	1695.2
Burning rate (g m^{-2} s^{-1})	3.756	3.996	4.008	3.984	6.552	7.224

Particle location	7	8	9	10	11	12	13
Temperature (K)	1695.2	1695.2	1695.2	1695.1	1695.1	1695.1	1695.1
Burning rate (g m^{-2} s^{-1})	7.272	6.876	6.204	5.484	5.208	5.316	5.832

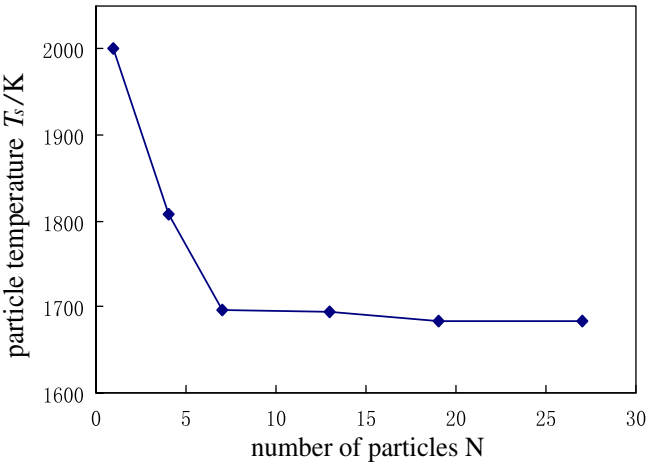

Fig. 17. Temperature variation of the center particle with different number of particles.

number of particles. At first, particle temperature decreases rapidly as the particle increases, and then it reduces to a certain value when the number is more than 7. This particle temperature variation trend is in agreement with the results discussed in Sections 4.2 and 4.3. When the number of particles is not more than 7, the O_2 supplied by the bulk gas is sufficient for char combustion, and the oxidization reaction I is the dominative reaction inside the cluster. Both the heterogeneous reaction I and homogeneous reaction III are exothermic reactions. With the particle increases, the O_2 supplied to each particle decreases, and the reacting rates of both two reactions decrease. Thus, the particle temperature decreases rapidly. However, when the number of particles is more than 7, the reaction rate of endothermic reaction II increases due to the lack of O_2. The particle temperature mainly depends on

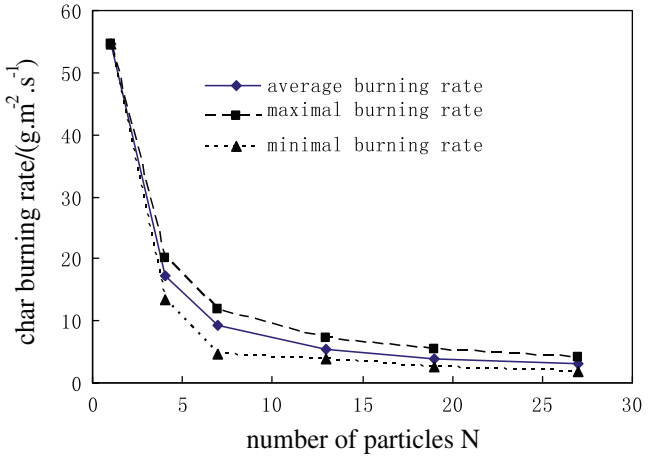

Fig. 18. Variation of char burning rate with different number of particles.

the endothermic reaction II and exothermic reactions III. With the number of particles increases further, the reacting rates of both two reactions increase and the particle temperature does not change evidently.

Table 3 also shows the char burning rate of each particle at the case of $N = 13$. The char burning rate of particle 1 which is located at the cluster center is the lowest, and that of particle 7 located at the foremost part (upstream) of the cluster is the highest. As discussed in Section 4.2, at the case of $N = 13$, since the particle cluster behaves as partial group combustion, the nine particles (No. 5–No. 13) located at the outer circle still burn individually, therefore their burning rates are much faster than those of the inner particles. However, because of the effects of convection, the particles located at the front part (upstream) of the cluster burn more quickly.

Fig. 18 shows the variation of char burning rate with different number of particles. At the case of $N = 1$, a single char particle burns in a hot oxidizing atmosphere, and the burning rate is up to 54.53 g/(m^2 s). With the increase of particles, the burning rate of each individual particle inside the cluster decreases. At the case of $N = 27$, the cluster average, maximum, and minimum burning rate are 2.99, 4.22, and 1.87 g/(m^2 s), respectively. In all simulated cases, the burning rate of the particle located at the foremost part of the cluster is the highest, and that of the particle located at the cluster center is the lowest.

5. Conclusion

In this paper, the micro-scale gas flow, heat transfer, and combustion processes occurred inside and around char clusters are studied. By contrastively studying the stable combustions of char particle clusters consisting of different number of particles, the combustion properties of char clusters in various particle concentrations are presented and discussed:

1. Under the simulation conditions in this paper, when particle concentration is very dilute, particles burn under the condition of isolated particle combustion. The quantities of O_2 and CO are relatively high around a single char particle, and the temperature difference between particle and flame caused by the combustion of CO is up to several hundred degrees Kelvin.
2. When the particles inside the cluster increase but are not more than 7, the O_2 mass fraction and the cluster temperature decrease. However, each particle inside the cluster still burns with its individual flame front. The char clusters behave as individual flame combustion.
3. When the particles inside the cluster are more than 7, the deoxidization reaction of CO_2 at inner particles' surface is strengthened. As the particles increase, the CO concentration inside the cluster increases and forms the CO combustion flame around the cluster. The flame temperature increases and the flame front expands. When the number of particles increases to 19 and more, the char cluster behaves as an individual large particle with pore surface. The gas temperature distributions within the cluster tend to be uniform.

4. The particle temperature decreases rapidly as the number of particles increases at first. It reduces to a certain value when the particles are more than 7.
5. The char burning rate decreases as the number of particles increases. In all the simulation cases, the burning rate of the particle located at the foremost part of the cluster is the highest, and that of the particle located at the cluster center is the lowest.

Acknowledgment

This work was supported by National Natural Science Foundation of China under Grant No. 50406025.

References

[1] F.C. Lockwood, T. Mahmud, M.A. Yehia, Simulation of pulverized coal test furnace performance, Fuel 77 (12) (1998) 1329–1337.
[2] R. He, T. Suda, T. Fujimori, et al., Effects of particle sizes on transport phenomena in single char combustion, Int. J. Heat Mass Transfer 46 (19) (2003) 3619–3627.
[3] K. Annamalai, S.C. Ramalingam, Group combustion of char/carbon particles, Combust. Flame 70 (3) (1987) 307–332.
[4] D.K. Zhang, T.F. Wall, Analysis of the ignition of coal dust cloud, Combust. Flame 92 (1993) 475–480.
[5] H. Katalambula, J. Hayashi, T. Chiba, et al., Dependence of single coal particle ignition mechanism on the surrounding volatile matter cloud, Energy Fuels 11 (1997) 1033–1039.
[6] B.R. Stanmore, Y.C. Choi, R. Gadiou, et al., Pulverized coal combustion under transient cloud conditions in a drop tube furnace, Combust. Sci. Technol. 159 (2000) 237–253.
[7] N. Takashi, Flame propagation in sprays and particle clouds of less volatile fuels, Combust. Sci. Technol. 177 (2005) 1167–1182.
[8] S. Krol, A. Pekediz, H.D. Lasa, Particle clustering in down flow reactors, Powder Technol. 108 (2000) 6–20.
[9] K. Tuzla, A.K. Sharma, J.C. Chen, et al., Transient dynamics of solid concentration in downer fluidized bed, Powder Technol. 100 (1998) 166–172.
[10] K.S. Lim, J.X. Zhu, J.R. Grace, Hydrodynamics of gas–solid fluidization, Int. J. Multiphase Flow 21 (1) (1995) 141–193.
[11] K. Annamalai, W. Ryan, Interactive processes in gasification and combustion, Part I, Prog. Energy Combust. Sci. 18 (3) (1992) 221–295.
[12] K. Annamalai, W. Ryan, S. Dhanapalan, Interactive process in gasification and combustion – Part III: coal/char particle arrays, streams and clouds, Prog. Energy Combust. Sci. 20 (1994) 487–618.
[13] X.Y. Du, C. Gopalakrishnan, K. Annamalai, Ignition and combustion of coal particle stream, Fuel 74 (1995) 487–494.
[14] W. Shuyan, L. Huilin, Z. Yunhua, et al., Numerical study of coal particle cluster combustion under quiescent conditions, Chem. Eng. Sci. 62 (2007) 4336–4347.
[15] D.S. Dandy, H. Dwyer, A sphere in shear flow at finite Reynolds number: effect of shear on particle lift, drag, and heat transfer, J. Fluid Mech. 216 (1990) 381–410.
[16] J.A. Arthur, Reactions between char and oxygen, Trans. Faraday Soc. 47 (1951) 164.
[17] H. Borouchaki, P.L. George, Aspects of 2-D delauney mash generation, Int. J. Numer. Methods Eng. 40 (11) (1997) 1957–1975.
[18] S. Muzaferija, Adaptive finite volume method for flow predictions using unstructured mashes and multigrid approach, Ph.D. thesis, University of London, London, 1994.
[19] S.R. Mathur, J.Y. Murthy, A pressure-based method for unstructured mashes, Numer. Heat Transfer B 31 (2) (1997) 195–215.
[20] A. Makino, An approximate explicit expression for the combustion rate of a small char particle, Combust. Flame 90 (2) (1992) 143–154.
[21] G. Adomeit, W. Hocks, K. Henriksen, Combustion of a char surface in a stagnation point flow field, Combust. Flame 59 (3) (1985) 273–288.
[22] H. Yan, C. Heidenreich, D. Zhang, Mathematical modeling of a bubbling fluidized-bed coal gasifier and the significance of 'net flow', Fuel 77 (1998) 1067–1079.
[23] J.B. Howard, G.C. Williams, D.H. Fine, Kinetics of carbon monoxide oxidation in postflame gases, in: 14th Symposium (International) on Combustion, Pittsburg, 1973, p. 975.